Retention of selenium by calcium aluminate hydrate (AFm) phases under strongly reducing radioactive waste repository conditions

Rojo, H.; Scheinost, A. C.; Lothenbach, B.; Laube, A.; Wieland, E.; Tits, J.;

Originally published:

February 2018

Dalton Transactions 47(2018), 4209-4218

DOI: https://doi.org/10.1039/C7DT04824F

Retention of selenium by calcium aluminate hydrate (AFm) phases under strongly reducing conditions

*H. Rojo[1,2], A.C. Scheinost[3], B. Lothenbach[4], A. Laube[1], E. Wieland[1], J. Tits[1]**

[1]Paul Scherrer Institut, Laboratory for Waste Management, 5232 Villigen PSI, Switzerland

[2]Institute for Nuclear Waste Disposal, Karlsruhe Institute of Technology, Karlsruhe, Germany

[3]The Rossendorf Beamline at ESRF, Grenoble, France, and Institute of Resource Ecology, Helmholtz-Zentrum Dresden-Rossendorf, Dresden, Germany

[4]Laboratory for Concrete and Construction Chemistry, Empa, Dübendorf, Switzerland

Prepared for submission to Environmental Science and Technology

Key-words: AFm phases, layered double hydroxides, selenide sorption, reducing conditions, x-ray absorption spectroscopy

ABSTRACT: Safety assessment studies of future nuclear waste repositories carried out in many countries predict selenium-79 to be a critical radionuclide due to its presence in the anionic form resulting in weak retardation by most common rock minerals. This assumption, however, ignores its potential uptake by AFm phases, positively charged anion exchangers which are present in significant quantities in the cementitious materials used in artificial barriers. Here we report for the first time wet chemistry and spectroscopic data on the interaction of the most reduced selenium anion species, i.e. HSe^-, with two AFm phases commonly found in cement, monocarbonate (AFm-CO_3) and hemicarbonate (AFm-$OHCO_3$). Batch sorption experiments show that Se(-II) is retained much more strongly (R_d = 100±50 L kg^{-1}) by the hemicarbonate than by the monocarbonate (R_d = 4±2 L kg^{-1}). The cause of this different sorption behavior was elucidated by extended X-ray absorption fine-structure (EXAFS) spectroscopy, showing that Se(-II) is mainly intercalated in the larger and hence more accessible interlayer of the hemicarbonate (d-spacing = 0.82 nm), whereas most Se(-II) is sorbed by the anion exchange sites on the outer surfaces of the AFm platelets in the case of monocarbonate, where the interlayer space is less accessible due to the smaller d-spacing of 0.75 nm. EXAFS spectra of oxidation experiments further show that Se(-II) in the interlayers is better protected from oxidation than Se(-II) sorbed to the outer surfaces. The quantitative sorption data along with the molecular-scale processes obtained from this study provide crucial insight into the Se mobility in the cementitious near-field of a radioactive waste repository under reducing conditions.

INTRODUCTION

Selenium-79 is one of the critical radionuclides for the safety of radioactive waste repositories due to its long half-live ($t_{1/2}$ = $3.27 \cdot 10^5$ years) and its presence in the anionic form resulting in

weak retardation by many common near- and far-field minerals in low and intermediate level nuclear waste (L/ILW) repositories.[1] The assumption of weak retention adopted in most safety assessment studies, however, ignores the potential uptake by positively charged anion exchangers such as hydrated calcium aluminate phases (AFm phases) present in the cementitious materials used as artificial barrier in L/ILW repositories.[2-5] AFm phases are Ca, Al layered double hydroxides consisting of Ca(OH) octahedral sheets in which 1/3 of the Ca^{2+} ions are replaced by Al^{3+} ions, resulting in a positive structural permanent charge (e.g. Matschei and co-workers 2007).[6] This positive charge is compensated by the intercalation of anions in the interlayers. The anionic composition of AFm phases in cementitious materials is dominated by anions such as CO_3^{2-}, SO_4^{2-}, Cl^- and OH^- depending on the type of cement.[6] These interlayer anions are generally relatively weakly bound thus providing potential exchange sites for ^{79}Se anions. In addition to these interlayer anion exchange sites, AFm phases also possess a smaller number of ion exchange sites on their outer surfaces (mainly positively charged interlayer cleavage faces). AFm phases thus seem to provide significant immobilization potential for this critical radionuclide.

Under the alkaline reducing conditions expected to prevail in the cementitious near field of a L/ILW repository ($10 < pH < 13.3$; $-750mV\ (SHE) < E_h < -230\ mV\ (SHE)$)[7, 8], Se(IV), Se(0), Se(-II) are the predominant redox states and the aqueous Se speciation is dominated by anionic species SeO_3^{2-}, HSe^- and a series of polyselenides (Se_x^{2-}), mainly Se_2^{2-}, Se_3^{2-} and Se_4^{2-} (Supporting information (SI), Figure S1).[9] During the last decade, several studies have been conducted to unravel the sorption behavior of SeO_3^{2-} onto cementitious materials, including AFm phases.[10-14] Sorption of Se(-II), however, has been largely ignored by the scientific community in the past, as it is experimentally difficult to stabilize this element in the (-II) redox state. The

present study deals with the sorption of HSe^- onto two types of AFm phases, AFm-CO_3 and AFm-$OHCO_3$. These phases were chosen because they are expected to be among the most stable AFm phases in hardened cement paste in the presence of carbonate.[2] In this study, batch sorption experiments under controlled reducing conditions were combined with X-ray Absorption Spectroscopy (XAS) investigations to monitor the selenium oxidation state and to characterize the molecular structure of HSe^- retained by these AFm phases.

MATERIALS AND METHODS

Experiments were carried out in inert N_2 atmosphere gloveboxes (O_2, CO_2 concentration < 0.1 ppm). Solutions were prepared using pro analysis grade chemicals and high-purity deionized water (resistivity = 18.2 M cm) generated by a Milli-Q Gradient A10 System (Millipore, Bedford, USA). The MilliQ water was degassed by boiling and bubbling N_2 for at least 2 hours prior to use.

AFm synthesis and characterization. Pure calcium aluminate hydrate (AFm) phases ($[Ca_2Al(OH)_6][X^{n-}]_{1/n}\cdot(H_2O)_m$), X being CO_3^{2-}, OH^-) were synthesized following the procedures described by Matschei et al.[15] The S:L ratio of the resulting AFm suspensions was $2\cdot10^{-2}$ kg L^{-1} (batch sorption experiments) or 0.1 kg L^{-1} (XAS experiments). A pure AFm-HSe phase ($([Ca_2Al(OH)_6][HSe^-]\cdot(H_2O)_m$) was synthesized by stoichiometrically mixing C_3A and NaHSe obtained by electrochemical reduction of Na_2SeO_3 followed by equilibration on an end-over-end shaker for four weeks.

A portion of the AFm suspensions were centrifuged (1 hour at 90’000 g (max)). The supernatant solutions were decanted and the pastes were dried for approximately 2 weeks in an airtight box over N_2 atmosphere in equilibrium with a saturated $CaCl_2$ solution (RH = ~35%). Powder X-ray

diffraction (PXRD) measurements were carried out using an X'Pert Pro MPD diffractometer with CoK radiation (= 1.789 Å). PXRD data of the sample containing Se(-II) were collected using a BRUKER AXS D8 ADVANCE Bragg-Brentano diffractometer with CuKa radiation (= 1.54 Å). A low background airtight sample holder was used to reduce the risk of Se(-II) oxidation during the measurements.

Reduction of Se(IV) to Se(-II). $NaHSe^{-II}$ solutions were obtained by electrochemical reduction of 10^{-2} M $Na_2Se^{IV}O_3$ solutions in 1.0 M NaOH with the help of a standard three electrode electrochemical cell coupled with a VMP3 multichannel potentiostat (Bio-Logic, France) in constant potential mode (E_h = -1.29V (SHE)) (SI, section 2). UV-Vis spectrometry (Cary 6000i, Agilent Technologies, USA) which allows identification of the reduced Se species (HSe^- and Se_x^{2-}) in solution[16-18] was used to confirm the completeness of the reduction reaction (SI; Figure S3 and S4).

Sorption experiments. Se(-II) is extremely sensitive to oxidation. Therefore, sorption experiments were performed in electrochemical cells (140 ml polyacryl containers) implementing a fixed redox potential of -1.0V (SHE). This redox potential was chosen to ensure sufficiently strong reducing conditions to keep Se in the (-II) redox state without significant O_2 production at the anode through electrolysis of H_2O. The electrochemical setup was similar to the one used for the reduction of Se(IV) to Se(-II) (SI, section 2), while the high surface area reticulated vitreous carbon (RVC) working electrode was replaced by a cylindrical glassy carbon working electrode (Sigradur G, HTW, Tierhaupten, Germany)[19]. 10 mL freshly prepared AFm suspensions (S:L = 0.1 kg L^{-1}) were mixed with 85 ml degassed MilliQ H_2O and 5 mL of a Se(-II) solution labeled with ^{75}Se radiotracer ($t_{1/2}$ = 119.8 days) (Imatom GmbH, Switzerland) to obtain a final total Se concentration of $1.25 \cdot 10^{-4}$ M. The initial ^{75}Se activity amounted to at least

9 Bq/ml. The suspensions were vigorously stirred for up to 18 days. In the case of long term sorption experiments (for XAS investigations), 38 mL of a 0.1 kg L^{-1} freshly prepared AFm suspension (S:L = 0.1 kg L^{-1}) was mixed with 2 mL of a 0.05 M radiotracer-free HSe^- solution ($[HSe^-]_{final}$ = $2.5 \cdot 10^{-3}$ M) in polyallomere centrifuge tubes. To this suspension, 0.2 ml hydrazine (N_2H_4) (64%), a strong reducing agent (E_h^0 = -1.15 V), was added to preserve reducing conditions [20, 21] (see SI, section 3). The tubes were shaken on an end-over-end shaker for 30 days. Duplicate 5 mL aliquots were sampled from the ^{75}Se labelled suspensions for gamma counting (Packard Cobra model 5003 gamma-counter, Perkin Elmer, USA) to determine the total ^{75}Se activity involved in the sorption reaction. Phase separation was obtained either by centrifugation (1 h at 95000g (max)) in the case of the XAS samples or by filtration (PTFE Filters, pore size 0.2 μm, Perkin Elmer, USA) in the case of the experiments in electrochemical cells. Triplicate 5 mL samples were taken from the supernatant solutions and filtrates and analyzed by gamma counting (^{75}Se labeled samples). The pH of the supernatant solutions was measured with a Metrohm combined glass electrode. The redox speciation of Se in the supernatant solutions was verified with UV-vis spectroscopy.

The distribution coefficient, R_d ($L \cdot kg^{-1}$), was calculated as follows:

$$R_d = \frac{\{Se\}}{[Se]_{eq}} = \left(\frac{A_{solid}}{A_{eq}}\right) \cdot \left(\frac{V}{m}\right) = \left(\frac{A_{susp} - A_{eq}}{A_{eq}}\right) \cdot \left(\frac{V}{m}\right) (L \cdot kg^{-1}) \quad , \qquad (1)$$

where $\{Se\}$ and $[Se]_{eq}$ are the amount of Se sorbed (mol kg^{-1}) and the equilibrium Se(-II) concentration, respectively. A_{solid} is the radionuclide activity sorbed ($cpm \cdot L^{-1}$), A_{eq} is the radionuclide activity in the equilibrium solution ($cpm \cdot L^{-1}$), A_{susp} is the total radionuclide activity in suspension ($cpm \cdot L^{-1}$). V and m are the suspension volume (L) and mass of solid (kg).

X-Ray Absorption Spectroscopy (XAS). AFm-CO_3 phases and AFM-$OHCO_3$ phases loaded with Se(-II) were prepared as described in section 2.3 with Se loadings varying between ~$5 \cdot 10^{-3}$ mol kg^{-1} (~450 ppm) and ~$2 \cdot 10^{-2}$ mol kg^{-1} (~1800 ppm). Wet pastes obtained after centrifugation were filled into Kapton-covered polyethylene sample holders inside the glovebox, and then immediately flash-frozen in liquid N_2 (LN_2). One series of samples (labelled "-ox") was exposed to air during sample preparation. The frozen samples were transported in a LN_2 Dewar to the Rossendorf Beamline at ESRF (Grenoble, France). For the XAS measurements, the samples were rapidly transferred from the Dewar to a closed-cycle He cryostat operating at 10-15 K. X-Ray Absorption Near-Edge Structure (XANES) and Extended X-Ray Absorption Fine-Structure (EXAFS) spectra were collected in fluorescence mode at the Se-K edge (12658 eV) using a 13-element high-purity Ge detector (Canberra) and Rh-coated mirrors for rejection of higher-order harmonics. XANES and EXAFS data analysis was performed with standard procedures using WinXAS [23], after energy calibration against the L_3 edge of elemental Au (11919 eV) and correction for the deadtime of the fluorescence detector by an experimentally determined function using SixPACK [22]. The threshold energy (E_0) was defined as the first inflexion point of the absorption edge, determined as knot of the second derivate of the absorption coefficient. Extraction of the EXAFS function was conducted by a cubic-spline fit from 1 to 12 $Å^{-1}$ using the auto-spline function of WinXAS to determine the optimum number of splines. The k^3-weighted EXAFS function was then Fourier-transformed using a Bessel window with parameter 3 across the k-space from 1.0 to 12.0 $Å^{-1}$. The theoretical phase shifts and backscattering amplitudes for shell fit were obtained with FEFF8.2 [24], using crystal structures of suited crystalline references as given below. The shift in threshold energy (ΔE_0) was varied as a global parameter in the fit procedure.

RESULTS AND DISCUSSION

Characterization of the AFm phases. PXRD patterns of AFm phases are characterized by strong basal reflections (00l) at low angles allowing the determination of the basal spacing d(00l) being the thickness of one Ca-Al double hydroxide layer plus one interlayer. The d-spacings were found to vary with the type of anion present in the AFm interlayer: the d-spacing of AFm-CO_3 is significantly smaller (d(00l)=0.75 nm) than that of AFm-$OHCO_3$ (d(00l) = 0.82 nm) (SI; Figure S5). Both values are in good agreement with d-spacings found in the literature for these two AFm-phases.[25-27] The AFm-HSe^- phase has a d-spacing of 0.80 nm; i.e., slightly smaller than the d-spacing of AFm-$OHCO_3$ but significantly larger than the d-spacing of AFm-CO_3.

Wet chemistry studies. The uptake of HSe^- is fast on both AFm-CO_3 and AFm-$OHCO_3$ phases and sorption equilibrium is reached within three days (Figure 1a). AFm-$OHCO_3$ exhibits the highest affinity for HSe^- in these experiments (R_d = 100±50 L kg^{-1}) whereas in the case of AFm-CO_3 the affinity for HSe^- was found to be a factor 25 lower (4±2 L kg^{-1}). The stronger sorption of HSe^- onto AFm-$OHCO_3$ compared to AFm-CO_3 results in much lower Se aqueous concentrations in solution (~$4 \cdot 10^{-5}$ M in the case of AFm-$OHCO_3$ compared to $2 \cdot 10^{-3}$ M in the case of AFm-CO_3). The pH of the suspensions was found to be 11.6 for AFm-CO_3 and 12.1 for AFm-$OHCO_3$, respectively.

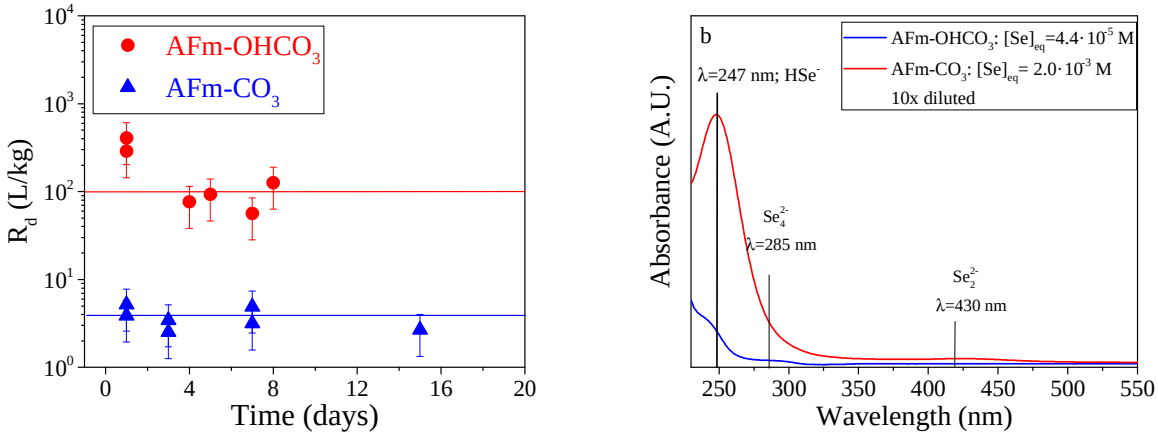

Figure 1. Kinetic studies of Se(-II) sorption on AFm-CO_3 and AFm-$OHCO_3$; $[Se]_{tot} = 1.08 \cdot 10^{-4}$ M. S:L = $1.11 \cdot 10^{-2}$ kg L^{-1}. a) R_d values; b) UV-Vis spectra of supernatant solutions of Se(-II) after 8 days equilibration.

UV-vis spectra of the supernatant solutions of the Se(-II) loaded AFm-CO_3 suspensions after 8 days equilibration confirm the (-II) redox state of the majority of the aqueous Se (Figure 1b). Only a very small shoulder may be observed at a wavelength of ~430 nm suggesting the presence of traces of Se_2^{2-}. This is however in contradiction with the Se redox speciation at pH = 11.5 predicting that at pH = 11.5, HSe^- oxidizes to Se_3^{2-} and Se_4^{2-} (See S.I., Figure S1). The UV-vis spectrum of the supernatant solution of the Se(-II) loaded AFm-$OHCO_3$ suspensions is characterized by a much lower absorbance due to the lower aqueous Se concentration. The clear shoulder at λ = 285 nm alongside the larger HSe^- shoulder at λ = 247 nm indicates that a significant part of the aqueous HSe^- has become oxidized to Se_4^{2-} in this sample: The low spectral intensities and the low resolution of this UV-Vis spectrum do not allow quantitative statements to be made about the aqueous redox speciation in this experiment. However, the presence of both HSe^- and Se_4^{2-} make the presence of the more strongly sorbing SeO_3^{2-} species[10] in the supernatant solutions of this experiment unlikely (see predominance diagrams in Figure

S1). The more pronounced HSe^- oxidation in the supernatant solution of the AFm-$OHCO_3$ suspension is explained by the lower Se concentration ($4.4 \cdot 10^{-5}$ M): assuming that only a small constant amount of oxygen is responsible for this oxidation effect, a higher fraction of the aqueous Se is oxidized in samples with low HSe- concentrations. The UV-vis spectra thus show that the electrochemical fixation of the redox potential in the experiment to a value of -1.2 V (SHE) could not completely prevent that part of aqueous Se was oxidized to polyselenides during the sorption experiment with AFm-$OHCO_3$. This oxidation of HSe^- to Se_4^{2-} might eventually explain the reduction of the R_d value with time for the Se sorption onto AFm-$OHCO_3$ observed in Figure 1a. The R_d values measured for HSe- sorption onto AFm-$OHCO_3$ thus represent the sorption of a mixture of HSe^- and Se_4^{2-} and should be taken only as an approximate R_d value for HSe^- sorption.

The difference in affinity for HSe^- of AFm-CO_3 and AFm-$OHCO_3$ may be explained by two factors: 1) The different binding mode of the CO_3^{2-} anions in the interlayer of both AFm phases resulting in a different interlayer distance, 2) Competition with CO_3^{2-} for anion exchange sites.

1) In AFm-CO_3, the main layer positive charge is fully compensated by CO_3^{2-} anions which are strongly retained by forming a direct bond to Ca ions in the main layers (interlayer carbonate anions share one oxygen with a Ca-O group of the main layer)[27, 28]. This makes the exchange of the interlayer CO_3^{2-} for other anions such as HSe^- very difficult. CO_3^{2-} thus effectively blocks the interlayer sites restricting HSe^- sorption to the positively charged outer planar surfaces of the AFm-CO_3 phases. In AFm-$OHCO_3$ on the contrary, the positive charge of the main layers is compensated by interlayer $[OH(CO_3)_{0.5}]^{2-}$ anions in which the CO_3^{2-} are only weakly bound by hydrogen bonds to the main layer[26]. This weaker bonding obviously facilitates the exchange of $[OH(CO_3)_{0.5}]^{2-}$ interlayer anions for HSe^-. Furthermore, the strongly bound CO_3^{2-} anions and the

water molecules in the interlayers of AFm-CO_3 firmly connect the main layers resulting in a rigid, narrow interlayer (basal spacing = 7.55 Å), hindering diffusion of other large anions such as HSe^- into the interlayer [27, 29]. The weakly bound $[OH(CO_3)_{0.5}]^{2-}$ anions in AFm-$OHCO_3$, however, give rise to much larger, more flexible interlayers (basal spacing = 8.2 Å. SI; Figure S5) allowing easy access to other large anions. The basal spacing of a pure AFm-HSe^- phase was found to be 7.97 Å (SI; Figure S5) suggesting that the interlayer of AFm-$OHCO_3$ is sufficiently large for HSe^- anions to occupy anion exchange positions.

2) In addition, the higher aqueous CO_3^{2-} concentration in the AFm-CO_3 suspensions (AFmCO_3: $[CO_3^{2-}] = 8 \cdot 10^{-6}$ M, AFm-OH-CO_3: $[CO_3^{2-}] = 3 \cdot 10^{-8}$ M)[30] may reduce HSe^- sorption through stronger competition.

X-Ray Absorption Spectroscopy (XAS). XAS analysis was carried out on AFm-CO_3 and AFm-$OHCO_3$ samples with Se(-II) loadings of ~450 ppm (AFm-CO_3) and 1800 ppm (AFm-$OHCO_3$), respectively. The equilibrium Se(-II) concentrations in these experiments was $\sim 2.5 \cdot 10^{-4}$ M in the case of the experiment with AFm-CO_3 and $< 10^{-5}$ M in the case of the experiments with AFm-$OHCO_3$. The Se redox speciation in the supernatant solutions was not checked, but, based upon the insights obtained from the wet chemistry experiments outlined in the previous section we can assume that after 1 month equilibration, the majority of the aqueous Se still was present as HSe^- in the experiment with AFm-CO_3, whereas in the experiments with AFm-$OHCO_3$ a large portion of the aqueous Se may have been oxidized.

Figure 2 shows the XAS spectra of HSe^- sorbed onto AFm-CO_3 (MC450) and onto AFm-$OHCO_3$ (HC1800) (in red), in comparison to the spectra of red Se(0) and the HSe^- aquo complex (in gray). The XANES spectra (Figure 2a) of MC450, HC1800 and an aqueous HSe^- solution all

show a similar white line position, which is at higher energy than the white line position of Se(0). While this would suggest a Se oxidation state higher than 0 at first glance, a comparison of the references shown in Figure 4a and previous publications [31, 32] reveal a sharp white-line feature for Fe selenides at about the same energy or even slightly below that of Se(0). This feature is also clearly present in the onset of the XANES edges of MC450 and HC1800, and to a lesser degree in the onset of the XANES of HSe^-. Its left-wing inflexion reveals an edge energy of 12650 eV (Table 1), ~5 eV below the edge energy of Se(0) compounds, thereby confirming the (-II) oxidation state of the Se sorbed on both AFm phases notwithstanding the partially higher oxidation state of the Se in the supernatant solutions (see above). HSe^- sorption onto both AFm phases thus appears to stabilize the (-II) oxidation state.

Since the shape of the Se(-II) XANES spectra is highly sensitive to the local coordination environment, the similarity of the XANES spectra of MC450, HC1800 and HSe^- already indicates that the coordination environment of all three species is similar. This is confirmed by the EXAFS spectra: all Fourier Transform Magnitudes (FTM) (Figure 2c) show a backscattering contribution at ~2.8 Å (uncorrected for phase shift). The corresponding k^3-weighted chi-spectra (Figure 2b) show that the main frequency has an amplitude maximum at a low k-value of ~3 $Å^{-1}$, which is typical for low-z elements like O. In contrast, Se compounds with Se next neighbours have an amplitude maximum at much higher k-values, as revealed by the chi-spectrum of red Se(0) (Figure 2b). We therefore assumed that Se(-II) in HSe^-, AFm-CO_3 and AFm-$OHCO_3$ is surrounded by water molecules at relatively long distances. For example in the highly hydrated Se(-II) compound $Na_2Se{\cdot}9H_2O$, Se(-II) is surrounded by 12 water molecules, with Se-O distances between 3.31 and 3.56 Å.[33] Using this structural information to calculate theoretical backscattering paths with FEFF8.2 and applying EXAFS shell fitting, we obtained for HSe^- a

similar coordination environment with ~12 O atoms at an average distance of 3.36 Å (Table 1). The relatively high Debye-Waller factor of 0.0106 $Å^2$, determined at a temperature of ~15 K where thermal contributions are considered to be negligible, suggests a relatively wide (static) distribution of Se-O distances as previously observed for $Na_2Se·9H_2O$. No statistically significant paths beyond this first water shell could be fitted for HSe^-. Additional neighboring atoms were observed for the MC450 and HC1800 samples: the FTM's show not only a strong backscattering contribution at ~2.8 Å, but also additional backscatterers at 4.7 and 6.8 Å distance (not phase shift corrected), suggesting structural order beyond the first coordination sphere.

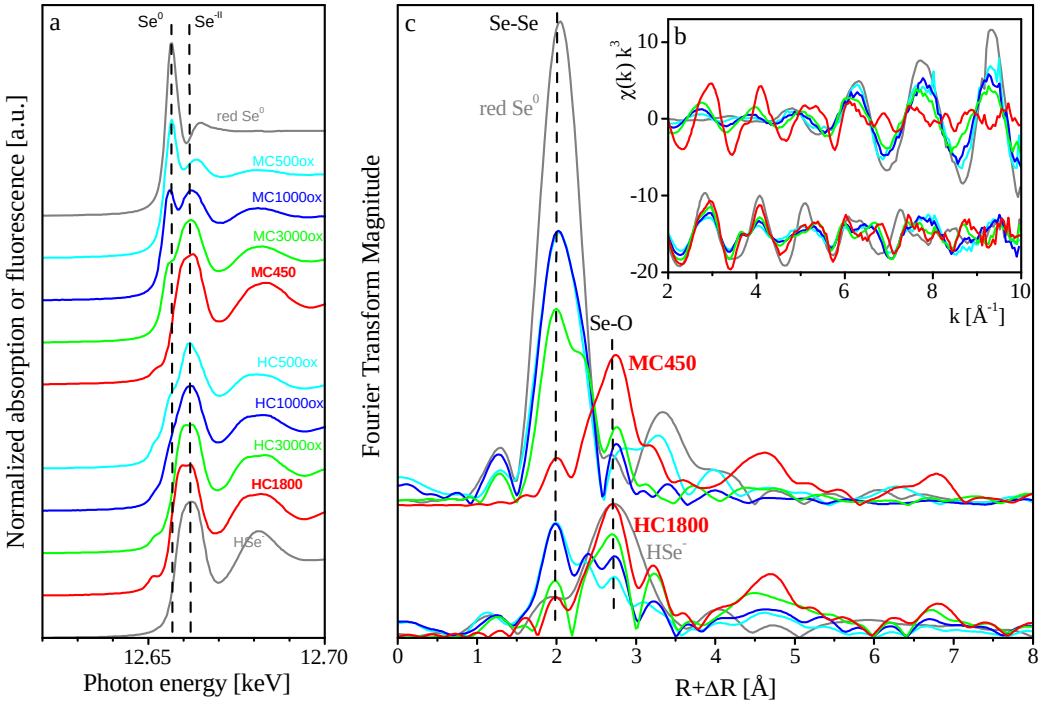

Figure 2. Se-K edge XAS spectra of Se-sorbed AFm-CO3 (MC, red top) and AFm-$OHCO_3$ (HC, red bottom) along with their respective oxidation series (blue->green->orange). The spectra

of red Se(0) and of HSe^- are shown in gray. XANES (left), EXAFS Fourier Transform Magnitude (right) and k^3-weighted $\chi(k)$ spectra (insert).

Table 1. Se-K XANES edge energies and EXAFS fit results of AFm samples and selected references. Crystallographic values of hydrocalumite as reference for HSe^- in HC1800 [34], of $Na_2Se\ 9H_2O$ as reference for the HSe^- aquo complex[33] and of red Se [35] are given in brackets.

Sample	**E_0 [eV]**	**Coordination shell**			**Further shells**			ΔE_0 [eV]	$\chi^2_{res\ \%}$
		CN	R [Å]	σ^2 [Å^2]	CN	R [Å]	σ^2 [Å^2]		
HC1800	12650.3	6^fO	3.28	0.0047	2.0 Ca	4.41	0.0121	4.1	19.0
			(3.41)		(2)	(4.51)			
		6^fO	3.49	0.0062	6.8^cCa	4.65	0.0150		
			(3.45)		(6)	(4.70)			
					6.8^cAl	5.27	0.0070		
					(6)	(5.13)			
MC450	12650.4	6^fO	3.25	0.0052	0.6 Ca	4.38	0.0120	3.5	18.1
		6^f O	3.43	0.0065	4.8^cCa	4.60	0.0128		
					4.8^c Al	5.21	0.0059		
HSe^-_{aquo}	12650.5	12.4 O	3.36	0.0106				3.1	11.7
		(12)	(3.31-3.56)						
red Se^0	12655.6	2 Se	2.36	0.0026	4.9 Se	3.73	0.0076	13.5	17.7
			(2.33)		(5)	(3.66-3.82)			
					4.1 Se	3.92	0.0100		
					(4)	(3.83-3.99)			

CN: coordination number with error ± 25 %, R: Radial distance with error ±0.01 Å, σ^2: Debye-Waller factor with error ±0.0005 Å^2, f: values fixed during fit, c: value correlated during fit.

For HC1800 with its larger d-spacing of 8.20 Å and the high HSe^- loadings, it is considered that HSe^- sorption may occur at least partially through the replacement of the $[OH(CO_3^{2-})_{0.5}]^{2-}$ unit in the interlayer space. HSe^- is likely to adopt a similar local coordination as Cl^- in AFm-Cl_2, given their similar charge and ionic radius (Figure 3)[34]. At this 3(b) site of the rhombohedral R-3 space group, Cl^- is located on top of a 7-coordinated Ca polyhedron (blue), which is surrounded by three other 7-coordinated Ca polyhedra (blue) and three Al octahedra (red, Figure 3 right). Bonding takes place through 3 OH groups (light blue spheres), which are each triply coordinated to two Ca polyhedra and one Al octahedron, and through 3 H_2O groups (purple spheres), which

form the apical corners of the Ca polyhedra protruding into the interlayer space. Since Cl^- in the interlayer binds to the double-hydroxide layers on both sides in exactly the same way, Cl^- is coordinated to 3 O atoms at 3.41 Å (H_2O), to 3 O atoms at 3.45 Å (OH groups), to 2 Ca atoms at 4.51 Å (axial Ca atoms directly above and below), to 6 Ca atoms at 4.70 Å, and to 6 Al atoms at 5.13 Å (Table 1). In the process of developing a structural model, we replaced Cl by Se and calculated the theoretical XAFS paths with FEFF8.2. Fitting this model to the HC1800 spectrum only two constraints had to be considered to achieve a statistically reliable fit with physically consistent parameters: 1) A preliminary fit of the first FTM peak showed that two different Se-O paths are required to fit the split first FTM peak, although the distal differences in the original Cl model are below the XAFS resolution ($\pi/(k_{max}-k_{min})/2=0.14$ Å). The coordination numbers of both paths were close to 6 and were therefore fixed to 6 for the subsequent fits. 2) The coordination numbers of the longer Se-Ca path and the Se-Al path were kept correlated to account for the characteristic structure of the double-hydroxide layers (Figure 3 right). The resulting fit parameters are given in Table 1 along with the starting values of the hydrocalumite-based model. The Se-Ca and Se-Al coordination numbers for HC1800 are (within errors of ±25%) as expected for HSe^- in the interlayer space and bonding to both double-hydroxide layers. The first Se-Ca path is 2% shorter, the second Se-Ca path is 1% shorter, and the Se-Al path is 3% longer compared to the (very symmetrical) Cl position in AFm-Cl_2. This are relatively small deviations, which can be explained by a higher structural disorder of Se(-II) in AFm-$OHCO_3$, which is also in line with the relatively large Debye-Waller factors. Furthermore, the two Se-O distances differ by 0.21 Å, also indicating a more distorted local coordination of HSe^- bonding to the two layers. Despite the modest distortion of the local environment, coordination numbers and distances are fully in line with HSe^- sorbed in the interlayer space of AFm-$OHCO_3$.

While the XAFS spectra of HC1800 and MC450 samples appear quite similar (red spectra in Figure 2b), the shell fit carried out for MC450 based on the same fit approach as described above, produced small, but statistically significant differences. While the Se-O coordination is again split into two subshells with 6 oxygen atoms each, the average distance of both shells is 3.34 Å and hence 0.05 Å smaller than for HC1800. The distances of the Ca and Al shells are also slightly smaller (0.03, 0.05 and 0.06 Å). Thus, all data show a consistent contraction of the distances around Se by ~1%. Furthermore, the coordination numbers of the Se-Ca and Se-Al shells are consistently lower (0.6 for the short Se-Ca path and 4.8 for the longer Se-Ca and Se-Al paths). These smaller coordination numbers suggest that, in contrast to the HSe^- bonding in HC1800, a substantial portion of HSe^- in the MC450 sample is bound to the outer surfaces of the AFm-CO_3 phase forming a similar sorption complex as in the interlayer space, but with only one layer of Al and Ca atoms. This is in line with our conceptualized model presented before, that the smaller interlayer space of the AFm-CO_3 phase is not easily accessible for diffusion of HSe- from bulk solution. If we assume that HSe^- binds exclusively to the outer surface, however, coordination numbers of ~1 for the short Se-Ca path and ~3 for the subsequent Se-Ca and Se-Al paths would be expected. Note that the observed CN of 4.8 for the long Se-Ca and the Se-Al path is ~60% higher, hence above the error limit of 25%. Therefore, HSe^- does not seem to reside exclusively at the outer surfaces, but also partly in the interlayer space. Given the relatively high errors of CN, no attempt was made to estimate the ratio of Se in the interlayers vs. on outer surfaces from the coordination numbers. The 1% contraction of the local Se environment could either arise from the fact that HSe^- is more strongly bound to the surface atoms, or from the smaller interlayer space of AFm-CO_3, hence cannot be used to quantify the distribution between both sites.

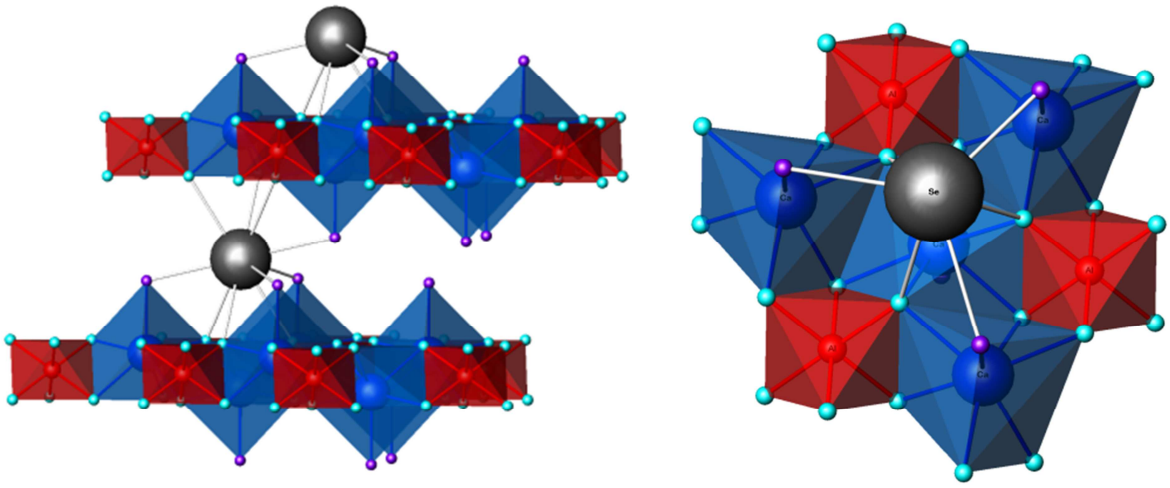

Figure 3. Hydrocalumite-based structural model of the EXAFS-derived positions of Se (gray spheres) in AFm-CO_3 and AFm-$OHCO_3$ (left : side view left, right : top view). HSe^- attaches to the surface Ca/Al double hydroxide layers through three OH-oxygen (light blue spheres) and three H_2O-oxygen atoms (purple spheres), forming edge-sharing complexes with four $Ca(OH)_7$ polyhedra (blue) and corner sharing complexes with 3 $Al(OH)_6$ octahedra (red) (right and top left). In the interlayer space, this coordination geometry is doubled since HSe^- is able to bind to the two adjacent layers in the same way (center left).

Further support for the sorption of a substantial fraction of Se(-II) onto the outer layers of AFm-CO_3 comes from the XAS spectra of the oxidation experiment (Figure 2). The XANES spectrum of the AFm-CO_3 sample with the highest Se loading (MC3000ox) shows a shoulder at the white position of Se(0), which grows into a distinct Se(0) white line with decreasing Se loading (MC1000ox and MC500ox). The increasing formation of Se(0) with decreasing Se loading is also shown by the EXAFS spectra (Figure 2b right). They reveal an increasing amplitude of the oscillations at high k-range in the EXAFs chi spectra, and an increasing peak at ~2 Å in the corresponding FTM in line with that of red Se(0) shown for comparison. Factor analysis in combination with an iterative target test [36, 37] using the spectra of MC450 and red Se(0) as pure

endmembers showed that samples MC3000ox, MC1000ox and MC500ox contain about 50, 70 and 80% of Se(0), respectively. The presence of Se(0) is much less pronounced in oxidized AFm-$OHCO_3$ samples as is evident from the XANES and XAFS spectra and from the iterative target test (5, 25 and 30% of Se(0) for samples HC3000ox, HC1000ox and HC500ox, respectively). Since Se(-II) bound in the interlayer space at high loadings is better protected against oxidation than Se(-II) bound onto the outer surfaces, this difference in degree of oxidation supports the structural interpretation given for the non-oxidized endmember spectra of the Se(-II) loaded AFm-$OHCO_3$ and AFm-CO_3 samples, that HSe^- in AFm-$OHCO_3$ sorbs predominantly in the interlayer space, while Se(-II) sorption onto AFm-CO_3 occurs predominantly on the outer surface due to limited access to the interlayer space.

IMPLICATIONS FOR RADIOACTIVE WASTE DISPOSAL

This study shows for the first time that the mobility of Se(-II) can be reduced significantly in the cementitious near field of a radioactive waste repository through sorption onto AFm phases such as AFm-CO_3 and AFm-$OHCO_3$. Se(-II) uptake by two carbonate containing AFm-phases was investigated; one with a large interlayer space (AFm-$OHCO_3$) and one with a smaller interlayer space (AFm-CO_3). Stronger sorption was observed onto the former AFm phase (R_d = 100±50 L kg^{-1}) whereas the sorption was significantly lower (R_d = 4±2 L kg^{-1}) on the latter AFm phase. EXAFS investigation showed that all Se(-II) was intercalated in the AFm interlayer of AFm-$OHCO_3$ whereas in the case of AFm-CO_3, Se(-II) was partially sorbed onto the outer AFm surface indicating that the smaller interlayer space of the AFm-CO_3 phase is not easily accessible for diffusion of HSe- from bulk solution. High carbonate concentrations favoring the formation of AFm-CO_3 can thus reduce the Se(-II) retention in the cementitious near-field of a radioactive waste repository.

ASSOCIATED CONTENT

Supporting information

The supporting information include a description of the Se redox speciation under alkaline conditions, a description of the experimental approach used for the reduction of Se(IV) to Se(-II), a short description of the reducing agent, hydrazine and PXRD data of the AFm phases. This material is available free of charge on the ACS Publications website at DOI:……...

AUTHOR INFORMATION

Corresponding author

*Phone: +41-56-310-4314; e-mail: jan.tits@psi.ch.

ACKNOWLEDGEMENT

This research was supported by the German Federal Ministry for Education and Research (grant 02NUK019A-IMMORAD) and by the Swiss Cooperative for the Disposal of Radioactive Waste (Nagra), Switzerland.

REFERENCES

(1) NAGRA *Project Opalinus Clay. Safety report. Demonstration of disposal feasibility for spent fuel, vitrified high-level waste and long-lived intermediate level waste (Entsorgungsnachweis)*; Nagra, Wettingen, Switzerland, 2002.

(2) Lothenbach, B.; Winnefeld, F. Thermodynamic modelling of the hydration of Portland cement. *Cem. Concr. Res.* **2006,** *36*, 209 – 226.

(3) Lothenbach, B.; Le Saout, G.; Gallucci, E.; Scrivener, K. L. Influence of limestone on the hydration of Portland cements. *Cem. Concr. Res.* **2008,** *38*, 848-860.

(4) Bullard, J. S.; Jennings, H. M.; R.A., L.; Nonat, A.; G.W., S.; Schweityer, J. S.; Scrivener, K. L.; Thomas, J. J. Mechanisms of cement hydration. *Cem. Concr. res.* **2011,** *41*, 1208 - 1223.

(5) Lothenbach, B.; Wieland, E. A thermodynamic approach to the hydration of sulphate-resistent Portland cement. *Waste Manage.* **2006,** *26*, 706-719.

(6) Matschei, T.; Lothenbach, B.; Glasser, F. P. The AFm phase in Portland cement. *Cem. Concr. Res.* **2007,** *37*, 118-130.

(7) Wersin, P.; Johnson, L. H.; Schwyn, B.; Berner, U.; Curti, E. *Redox Conditions in the Near Field of a Repository for SF/HLW and ILW in Opalinus Clay*; 2003.

(8) Berner, U. *Project Opalinus Clay: Radionuclide Concentration Limits in the Cementitious Near-Field of an ILW Repository*; PSI Bericht Nr. 02-26, Paul Scherrer Institut, Villigen, Switzerland and Nagra Technical report NTB 02-22, Wettingen, Switzerland; 2003; p 48.

(9) Olin, Å.; Noläng, B.; Osadchii, E. G.; Öhman, L.-O.; Rosén, E. *Chemical thermodynamics of Selenium*. Elsevier, Amsterdam: 2005; Vol. 7.

(10) Baur, I.; Johnson, C. A. Sorption of selenite and selenate to cement materials. *Environ. Sci. Technol.* **2003,** *37*, 3442-3447.

(11) Bonhoure, I.; Baur, I.; Wieland, E.; Johnson, C. A.; Scheidegger, A. M. Uptake of Se(IV/VI) oxyanions by hardened cement paste and cement minerals: An X-ray absorption spectroscopy study. *Cem. Concr. Res.* **2006,** *36*, 91-98.

(12) Zhang, M.; Reardon, E. J. Removal of B, Cr, Mo, and Se from wastewater by incorporation into hydrocalumite and ettringite. *Environ. Sci. Technol.* **2003,** *37*, 2947 - 2952.

(13) Johnson, E. A.; Rudin, M. J.; Steinberg, S. M.; Johnson, W. H. The sorption of selenite on various cement formulations. *Waste Manage.* **2000,** *20*, 509 - 516.

(14) Macé, N.; Landesman, C.; Pointeau, I.; Grambow, B.; Giffaut, E. Characterisation of thermally altered cement pastes. Influence on selenite sorption. *Adv. Cem. Res.* **2007,** *19*, 157-165.

(15) Matschei, T.; Lothenbach, B.; Glasser, F. P. Thermodynamic properties of Portland cement hydrates in the system $CaO–Al_2O_3–SiO_2–CaSO_4–CaCO_3–H_2O$. *Cem. Concr. Res.* **2007,** *37*, 1379 - 1410.

(16) Licht, S.; Fourouyan, F. Speciation analysis of aqueous polydelenide solutions. *J. Electrochem. Soc.* **1995,** *142*, (5), 1546-1551.

(17) Lyons, L. E.; Young, T. L. Alkaline selenide, polyselenide electrolytes: concentrations, absorption spectra and formal potentials. *Aust. J. Chem.* **1986,** *39*, 511-527.

(18) Ansari, M. A.; Ibers, J. A. Soluble selenides and tellurides. *Coord. Chem. Rev.* **1990,** *100*, 223-266.

(19) Soltermann, D.; Baeyens, B.; Bradbury, M. H.; Marques Fernandez, M. Fe(II) uptake on natural montmorillonites. II. Surface complexation modeling. *Environ. Sci. Technol.* **2014,** *48*, 8698-8705.

(20) Iida, Y.; Yamaguchi, T.; Tanaka, T.; Nakayama, S. Solubility of selenium at high ionic strength under anoxic conditions. *J. Nuclear Sci. Technol.* **2010,** *47*, (5), 431 - 438.

(21) Iida, Y.; Tanaka, T.; Yamaguchi, T.; Nakayama, S. Sorption behavior of selenium(-II) on rocks under reducing conditions. *J. Nuclear Sci. Technol.* **2011,** *48*, (2), 279 - 291.

(22) Webb, S. M. SIXPack: a graphical user interface for XAS analysis using IFEFFIT. *Physica Scripta* **2005,** *T115*, 1011-1014.

(23) Ressler WinXAS: a program for X-ray absorption spectroscopy data analysis under MS-Windows. *J. Synchrotron Rad.* **1998,** *5*, 118-122.

(24) Ankudinov, A. L.; Rehr, J. J. Relativistic calculations of spin-dependent x-ray-absorption spectra. *Phys. Rev B* **1997,** *56*, 1712-1728.

(25) Renaudin, G.; Francois, M.; Evrard, O. Order and disorder in the lamellar hydrated tetracalcium monocarboaluminate compound. *Cem. Concr. Res.* **1999,** *29*, 63-69.

(26) Runcevski, T.; Dinnebier, R. E.; Magdysyuk, O. V.; Pöllmann, H. Crystal structures of calcium hemicarboaluminate and carbonated calcium hemicarboaluminate from synchrotron powder diffraction data. *Acta Cryst.* **2012,** *B68*, 493-500.

(27) Francois, M.; Renaudin, G.; Evrard, O. A cementitious compound with composition $3CaO.Al_2O_3.CaCO_3.llH_20$. *Acta Cryst.* **1998,** *C54*, 1214-1217.

(28) Renaudin, G.; Mesbah, A.; Dilnesa, B. Z.; Francois, M.; Lothenbach, B. Crystal chemistry of iron containing cementitious AFm layered hydrates. *Current Inorganic Chemistry* **2015,** *5*, 184-193.

(29) Baquerizo, L. G.; Matschei, T.; Scrivener, K. L.; Saeidpour, M.; Wadsö, L. Hydration states of AFm cement phases. *Cem. Concr. Res.* **2015,** *73*, 143-157.

(30) Matschei, T. Thermodynamics of cement hydration. PhD thesis, University of Aberdeen, Aberdeen, U.K., 2007.

(31) Scheinost, A. C.; Charlet, L. Selenite reduction by mackinawite, magnetite and siderite: XAS characterization of nanosized redox products. *Environ. Sci. Technol.* **2008,** *42*, 1984–1989.

(32) Scheinost, A. C.; Kirsch, R.; Banerjee, D.; Fernandez-Martinez, A.; Zaenker, H.; Funke, H.; Charlet, L. X-ray absorption and photoelectron spectroscopy investigation of selenite reduction by FeII-bearing minerals. *J. Contam. Hydrol.* **2008,** *102*, 228-245.

(33) Bedlivy, D.; Preisinger, A. Die Struktur von $Na_2S \cdot 9H_2O$ und $Na_2Se \cdot 9H_2O$. *Zeitschrift für Kristallographie* **1965,** *121*, (2-4), 114-130.

(34) Rousselot, I.; Taviot-Gueho, C.; Leroux, F.; Leone, P.; Palvadeau, P.; Besse, J. P. Insights on the structural chemistry of hydrocalumite and hydrotalcite-like materials: Investigation of the series $Ca_2M^{3+}(OH)_6Cl\ x2H_2O$ (M^{3+}: Al^{3+}, Ga^{3+}, Fe^{3+}, and Sc^{3+}) by X-ray powder diffraction. *Journal of Solid State Chemistry* **2002,** *167*, (1), 137-144.

(35) Cherin, P.; Unger, P. Refinement of the crystal structure of alpha-monoclinic Se. *Acta Crystallogr., B* **1972,** *28*, 313-317.

(36) Rossberg, A.; Reich, T.; Bernhard, G. Complexation of uranium(VI) with protocatechuic acid - application of iterative transformation factor analysis to EXAFS spectroscopy. *Anal. Bioanal. Chem.* **2003,** *376*, 631-638.

(37) Charlet, L.; Scheinost, A. C.; Tournassat, C.; Greneche, J. M.; Gehin, A.; Fernandez-Martinez, A.; Coudert, S.; Tisserand, D.; Brendle, J. Electron transfer at the mineral/water interface: Selenium reduction by ferrous iron sorbed on clay. *Geochim. Cosmochim. Acta* **2007,** *71*, (23), 5731-5749.